PAPER

Check for updates

Nonconductive ferrofluids from permanently magnetic nanoplatelets hybridized with polar phosphonic ligands†

Ali Tufani,‡[a] Nina Popov,§[a] Janez Kovač,[a] Stanislav Čampelj,[a] Andraž Mavrič, [ID] [b] Tomáš Landovský,[c] Martin Cigl, [ID] [c] Petra Vaňkátová,[c] Martin Loula,[d] Vladimíra Novotná, [ID] [c] Matic Poberžnik,[a,e] Gabriela Herrero-Saboya,[e] Layla Martin-Samos,[e] Alenka Mertelj [ID] [a] and Darja Lisjak [ID] *[a]

Ferrofluids composed of permanently magnetic nanoplatelets of barium hexaferrite (BHF NPLs) represent a remarkable class of materials that can form a ferromagnetic liquid state at sufficiently high concentrations. To date, the surfactant dodecylbenzenesulfonic acid (DBSA) has demonstrated an excellent colloidal stability of the BHF NPLs in alcohols. However, a key limitation of DBSA is its labile adsorption onto the NPLs, meaning that the surface coverage by surfactant molecules is highly sensitive to various factors. In this study, we demonstrate that polar ligands based on phosphonic acids and phosphonate esters offer a viable alternative to DBSA, providing enhanced robustness and colloidal stability in low-polar solvents. Phosphonic ligands with the different electron-withdrawing groups and alkyl chain lengths of the terminal chain and linker were synthesized. Their attachment to the surface of the BHF NPLs was studied for various conditions and followed by a combination of spectroscopic techniques, thermogravimetry, and electrokinetic measurements. The results confirmed the theoretically predicted surface condensation of the ligands onto the BHF NPLs surfaces at 120 °C in 1-hexanol, whereas at lower temperatures or in more polar solvents the ligands were mostly physisorbed. The NPL hybrids with chemisorbed ligands having surface densities of at least 0.4 molecules per nm^2 formed stable ferrofluids in 1-hexanol. Due to the relatively low polarity of 1-hexanol, the ligands remain protonated and the ferrofluids have negligible electric conductivity and are suitable for the development of novel magneto-optic sensors that can operate under an electric field.

Introduction

Until recently, two types of magnetic fluids, *i.e.*, magnetorheological fluids and ferrofluids, were studied and exploited for various applications, such as magnetic dampers and seals, magnetic separation, and in biomedicine.[1–4] Both types of

[a]Jožef Stefan Institute, Jamova 39, SI-1000 Ljubljana, Slovenia.
E-mail: darja.lisjak@ijs.si
[b]University of Nova Gorica, Materials Research Laboratory, Vipavska 13, SI-5000
Nova Gorica, Slovenia
[c]Institute of Physics of the Czech Academy of Sciences, Na Slovance 2, 182 00 Prague
8, Czechia
[d]Institute of Organic Chemistry and Biochemistry of the Czech Academy of Sciences,
Flemingovo náměstí 2, 166 10, Prague 6, Czechia
[e]CNR-IOM, Democritos National Simulation Center, Istituto Officina dei Materiali,
c/o SiSSA, IT-34136 Trieste, Italy

‡Now with University of Padova, Department of Industrial Engineering, Via Marzolo 9, 35131 Padova, Italy.
§Now with Ruđer Boskovic Institute, Bijenicka cesta 54, 10 000 Zagreb, Croatia.

magnetic fluids consist of highly magnetizable particles in a carrier liquid. These ferrofluids are stable colloids of superparamagnetic nanoparticles. The nano-size and lack of remanent magnetization enable the colloidal stabilization of superparamagnetic nanoparticles by tuning their surface chemistry and the solvent's properties like in any other nanoparticulate system. In particular, due to the nano size, they are not affected by gravity and, due to the lack of remanent magnetization, they do not experience relatively long-range magnetic dipolar attraction as in the case of permanently magnetic particles. The magnetorheological fluids consist of magnetically similar but larger soft magnetic microparticles. Since these particles possess very low remanent magnetization, the magnetic dipole interaction between them is very weak or negligible in a zero magnetic field. Consequently, such particles can be suspended in a carrier liquid, *i.e.*, similar to any other nonmagnetic particles affected by gravity.

The first stable dispersions, *i.e.*, ferrofluids, of permanently magnetic nanoparticles were reported more than a decade ago.[5] In these ferrofluids, ferrimagnetic barium hexaferrite nanoplatelets (BHF NPLs) were stabilized in alcohols (*i.e.*,

from methanol to hexanol). The long-range magnetic dipolar attraction between the NPLs was successfully suppressed by a long-range electrosteric interaction induced by an amphiphilic surfactant, dodecylbenzenesulfonic acid (DBSA). The excellent colloidal stability of these systems enabled the development of the first ferromagnetic ferrofluid.[6] In the highly concentrated (*i.e.*, 28 vol%) ferrofluids of the BHF NPLs in 1-butanol, the NPLs are ferromagnetically coupled. Subsequently, the first known room-temperature liquid magnet with a fully evolved ferromagnetic domain structure in the remanent state was prepared in the same colloidal system.[7] Each ferromagnetic domain in this ferromagnetic ferrofluid is composed of regions with ferromagnetically aligned BHF NPLs. Alternative hexaferrite ferrofluid systems are aqueous,[8,9] however, with limited concentrations of NPLs.

Possible applications based on the known BHF-NPLs ferrofluids, such as sensors and photonic elements, rely on a magneto-optic effect;[10–12] however, they cannot be used under an applied electric field. This limitation arises from a conducting carrier solution prone to an electric breakdown under an applied electric field. The solutes in relatively highly polar solvents, such as 1-butanol or other shorter alcohols (C3–C6), can dissociate, and the ions forming a double layer around the surface-charged BHF NPLs are in equilibrium with the ions in the bulk liquid.[13] In contrast, an electric field can be applied in solvents with relatively low polarity, in which the solutes cannot dissociate. Consequently, the particles' surfaces cannot dissociate either. In such systems, the particles should be stabilized through non-electrostatic repulsive interactions (*e.g.*, steric and/or solvation).[14] The first reported BHF ferrofluids were prepared in an apolar solvent from superparamagnetic BHF nanoparticles with poor magnetic properties.[15,16] Scarce reports[17–19] suggested that ferrofluids of permanently magnetic BHF NPLs can also be obtained in nonpolar solvents. However, the proposed systems were obtained in highly viscous (silicon oil and paraffin) or volatile (chloroform) solvents that, in both cases, limit their applications. The response time to an applied magnetic field increases with the solvent's viscosity and limits possible applications of such ferrofluids. On the other hand, a special chemically stable and super-tight casing is required for chloroform. In this study, we aimed to overcome the above limitations using an alternative, non-volatile solvent of sufficiently low polarity to ensure electrical insulation. At the same time, we had to tailor the surface chemistry of the BHF NPLs to disperse them in a low-polar solvent.

The interparticle interactions and the interactions of particles with a solvent depend on the particles' surface properties, which can be tuned by functionalizing or hybridizing the particles' surfaces with organic ligands. An intuitive solution for a colloidal system lacking electrostatic repulsion would be to functionalize the particles' surfaces with a dense layer of sterically repelling ligands, such as self-assembled monolayers (SAMs).[20–22] SAMs are used in various applications, including corrosion inhibition, antifogging, and self-cleaning materials. The ligands attach to the surfaces of metal oxides *via* different binding interactions, *i.e.*, covalent, coordinative, and physical interactions, such as a hydrogen bond, van der Waals, and electrostatic interactions.[23–25] The binding interaction depends on the ligand's anchoring group and the surface chemistry of the particles.[20,22,23,26,27] Among these, the irreversible attachment is ensured only through the covalent interaction, while the stability of the other interactions is system-dependent (*e.g.*, on the pH, temperature, solution composition).

The phosphonate moieties are excellent anchors for metal–oxide surfaces.[23,28–30] Some studies suggest a possible covalent binding[23,28,31,32] between a phosphonate moiety with the surface of a metal (M) oxide forming the M–O–P bonds by condensation of the P–OH groups with the surface OH groups (Scheme 1). In addition, the P=O group can coordinate with the surface metal atoms.[32,33] The interaction of the phosphonic moieties with the metal atoms depends on the nature and oxidation state of the surface metal, the backbone of the phosphonic ligand, and the reaction conditions (temperature, pH, *etc.*). Therefore, the phosphonic ligands can also assemble randomly or in several layers on metal–oxide surfaces *via* coordinative, hydrogen, electrostatic, and/or van der Waals interactions.[28,34,35]

The surface functionalization of the BHF NPLs with some phosphonic ligands resulted in stable aqueous dispersions.[34] All these phosphonic acids contained an additional charge-
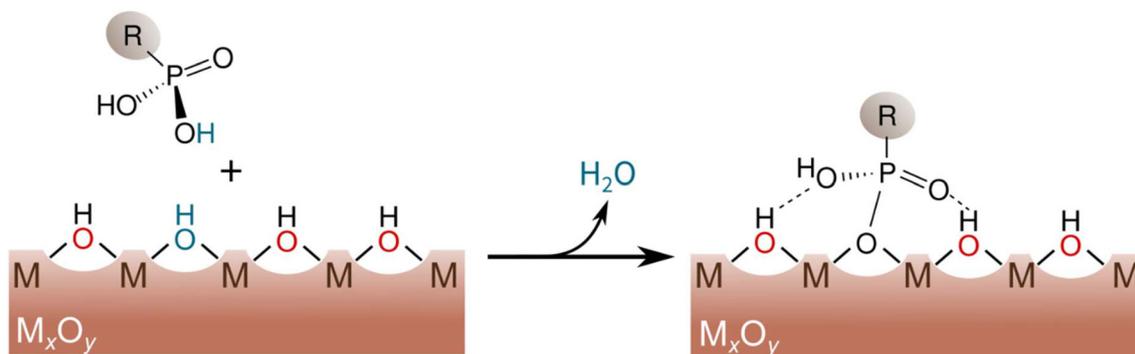
Scheme 1 Schematic representation of the condensation reaction between a phosphonic ligand and a metal (M) oxide surface that results in a monodentate bonded phosphonate ligand.
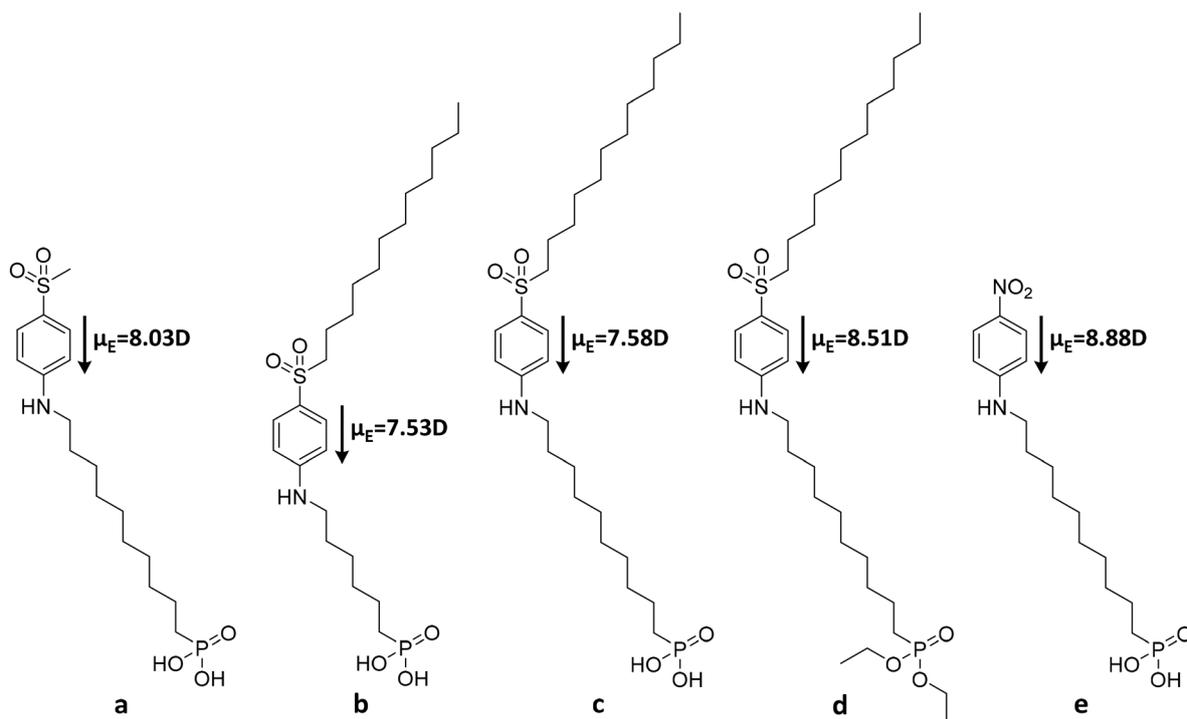
Chart 1 Phosphonic ligands used for hybridizing the BHF NPLs with the calculated dipole moments μ_E.

bearing group (*i.e.*, sulfonic or additional phosphonic group), ensuring the electrostatic repulsion. However, the free charge-bearing group can interact with the unbound ligands, enabling the formation of bi- or multiple layers on surfaces. In contrast, monophosphonic acids and phosphonic esters favour SAMs.[36,37] Since their only charge-bearing group is the anchoring phosphonic group, they do not provide the needed electrostatic repulsion for stabilizing the particles in polar solvents. On the other hand, they are suitable for stabilizing the particles in weakly polar or apolar solvents.[38–40]

In our study, we designed monophosphonic acids and an ester containing a polar push-pull system but no additional charge-bearing group (Chart 1). We hypothesized that such ligand structures would form SAMs on metal oxide surfaces and would, at the same time, colloidally stabilize the BHF NPLs in weakly polar solvents *via* a repulsive interaction between the surface dipoles. The ligands' structures varied with respect to the electron-withdrawing group (*i.e.*, sulfonyl or nitro), the length of the terminal alkylsulfonyl chain, and the length of the amino–phosphono alkyl linker. In this way, we varied the ligands' polarities and solubilities in different solvents. By optimizing the functionalization conditions, we obtained stable phosphono-BHF nanohybrids that were dispersible in 1-hexanol.

First-principles calculations

The electric dipole moments of the synthesized ligands in the gas phase were calculated with the Gaussian 16 package for electronic

structure calculations.[41] All calculations were performed with the PBE functional[42] and the def2-TZVPP basis set.[43] The structures were geometrically optimized. We found that the estimated electrical dipole moment is sensitive to small variations in the atomic positions. In particular, we observed that the relative orientation of the phosphonate anchor group with respect to the polarisable backbone can modify the electrical dipole moment up to 1 D. The electrical dipoles in Chart 1 correspond to the lowest energy configurations.

The density-functional theory (DFT) modelling of the adsorption of phosphonic acids onto the BHF NPLs was described in detail in our previous publication.[44] Here, only the main conclusions are summarized. We characterized the adsorption of a simplified phosphonate-based ligand ($CH_3PO_3H_2$) on a periodic slab model of the fully hydroxylated 12k-O surface of BHF. This model is considered representative of the adsorption of phosphonic acids onto the BHF NPLs, as the fully hydroxylated 12k-O surface is the most favourable bulk termination in media having at least traces of water[45] and the ligand backbones govern lateral interactions in the monolayer and should not affect the mechanism of adsorption. Two adsorption modes were considered, designated as plain adsorption and adsorption *via* condensation. In the first mode, the ligand is adsorbed by forming hydrogen bonds with surface OH groups. In the second mode, a surface OH group is replaced by the ligand and a water molecule forms as a side product (as in Scheme 1). For both modes, we estimated the Gibbs free energy of adsorption (ΔG_{est}) by taking into account the decrease in entropy due to the loss of translational and

rotational degrees of freedom upon adsorption.[44] The obtained $\Delta G_{est} = -0.25$ eV for the physisorption and $\Delta G_{est} = -0.58$ eV for the chemisorption suggest that both processes are thermodynamically possible, although condensation is preferred. Despite a possible covalent contribution to the hydrogen-bond interaction,[46] the hydrogen bond will be considered in this contribution, similar to a general understanding, as a physical interaction of ligands with a solid surface, *i.e.*, physisorption. Meanwhile, adsorption *via* condensation is correlated to chemisorption, *i.e.*, covalent or coordinative interaction. Finally, we also considered the formation of an additional bond *via* the condensation mechanism, since the bidentate (or even tridentate) bonding mode is often proposed in the literature.[31] However, our results indicate that the formation of a second strong bond *via* condensation is unfavourable, with an exergonic ΔG_{est} of 0.3 eV (see Fig. S1 in the ESI†). This indicates that on a defect free, fully hydroxylated surface, phosphonate ligands are bonded in the monodentate bonding mode.

We can also deduce the maximum surface density of a ligand in terms of the steric footprint of the phosphonate group.[47] Given that only one phosphonic ligand can be adsorbed per unit cell (see Fig. 1) and the area of the unit cell is 0.31 nm^2, we can propose an upper limit for the number of adsorbed phosphonic groups on the surface when forming a monolayer to about 3–4 ligands per nm^2.

Keeping the above results in mind, we studied the: (i) conditions ensuring the condensation reaction, *i.e.*, stable hybridization between the BHF NPLs' surfaces and the phosphonic ligands (Chart 1) and (ii) the preparation of ferrofluids from the hybrid BHF NPLs in nonconductive solvents.

Experiment and characterization methods

Chemicals

Barium(II) nitrate (99.95%), iron(III) nitrate nonahydrate (>98%), scandium(III) nitrate hydrate (99.9%), nitric acid (65%), NaOH (98%), methanol and 1-hexanol were obtained from Alfa Aesar. The contents of the metals in the respective salts were determined with inductively coupled plasma optical emission spectroscopy (ICP-OES, Agilent 5800 VDV). The chemicals used in the organic synthesis of the polar ligands were obtained from Merck and Fluorochem, see ESI† for details.

Synthesis of the barium hexaferrite nanoplatelets (BHF NPLs)

BHF NPLs were synthesized hydrothermally with the partial substitution of Fe^{3+} with Sc^{3+}.[48] 25 mmol of Ba, Fe, and Sc nitrates in the molar ratio Ba : Fe : Sc = 1.0 : 4.5 : 0.5 were dissolved in 200 mL water and 200 mL of aqueous sodium hydroxide (1.13 mol) was added to the solution. The solution was transferred to a sealed Inconel autoclave (1 L, Parr Instruments) and then heated to 240 °C with a heating rate of 3 °C min^{-1} followed by natural cooling to ambient temperature. The synthesized NPLs were washed with deionized (DI) water to remove the unreacted solutes and then with 0.1 mol L^{-1} nitric acid to remove the barium carbonate side product. Finally, the washed BHF NPLs were dispersed in the nitric acid solution at a pH of 1.7.
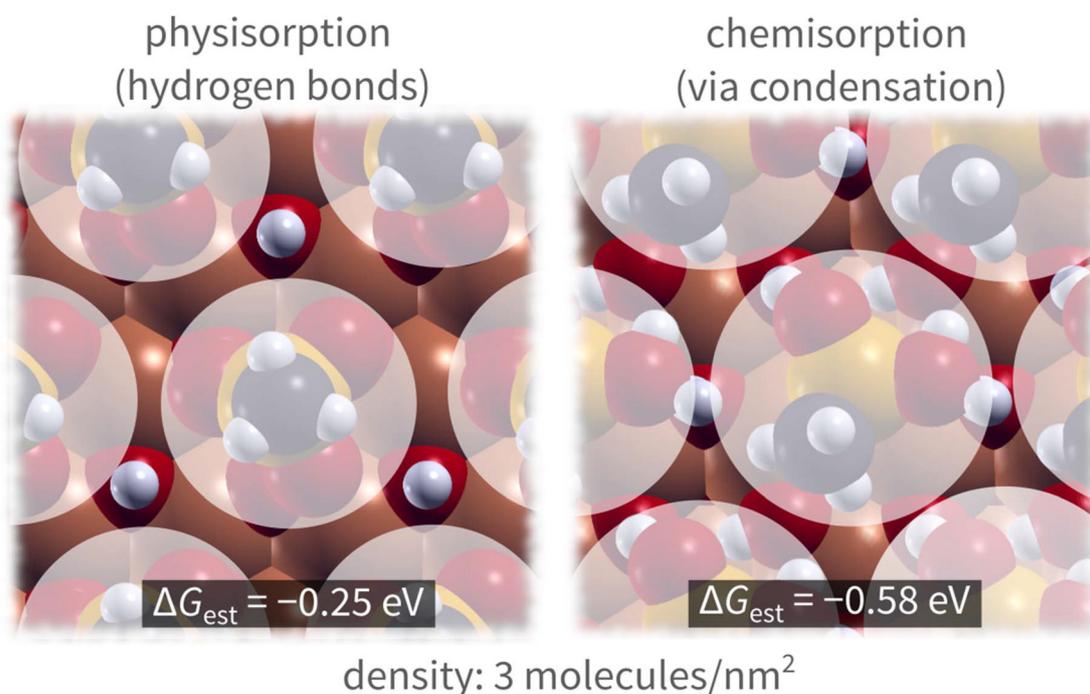

Fig. 1 Top views of the adsorption of the $CH_3PO_3H_2$ ligand in the two considered adsorption modes. Note that adsorbing additional ligands would lead to steric hindrance between the ligands within the semi-transparent white circles.

Synthesis of polar ligands

Both types of polar ligands (phosphonic acids a–c, e; and diethyl phosphonate d) were synthesized using a similar protocol, using various combinations of smaller building blocks (Scheme 2, see ESI† for details). While ligands a and d were prepared as pure compounds, the rest of the phosphonic acids b, c, and e were isolated and further used in the form of hydrobromic salts. The final purity of the ligands was roughly 80–100% (Table S1 in ESI†). The HBr was washed away during the hybridization of the NPLs, as was confirmed with various analytical techniques used to characterize the hybrids. No evidence of HBr or Br⁻ was detected with X-ray photoemission (XPS), infrared (IR), and mass spectroscopies.

## Hybridization of the BHF NPLs with phosphonate ligands

We investigated the conditions for a robust attachment, *i.e.*, the hybridization of phosphonic ligands (Chart 1), onto the BHF NPLs *via* a condensation reaction (Scheme 1). Firstly, the BHF NPLs (~85 mg) were transferred from the aqueous phase (4 mL) to the selected solvent (100 mL), *i.e.*, methanol or 1-hexanol. The hybridization was conducted under reflux by the dropwise addition of the ligand solution (3 mL) in the selected solvent followed by stirring for 3 hours. The nominal ligand concentration was adjusted roughly to 3 (*i.e.*, approximately for a monolayer; see the Calculations section) or 10 molecules per nm^2 of the NPL surfaces (see details in ESI Table S1†). The reaction temperature was set to 50, 80, or 120 °C. The hybridized NPLs were washed with the hybridiz-

ation solvent and dispersed in different solvents. An additional sample was prepared at 250 °C, similar to the others, but the heating step was performed in an autoclave. The summary of the hybridization conditions is listed in Table 1. All the ligands were soluble in methanol but insoluble in apolar solvents, such as toluene and *p*-xylene. As an alternative solvent with intermediate polarity, we chose 1-hexanol (see ESI† for the selection procedure). The solubility of the ligands in 1-hexanol was ≥1 mmol L⁻¹, which was high enough to reach the required concentration in the reaction mixture. An exception was ligand b, which was only soluble in methanol. Therefore, its hybrids were only prepared in methanol.

Characterization methods

Bare and hybridized NPLs were analysed with a transmission electron microscope (TEM, Jeol 2100, Tokyo, Japan) coupled with an energy-dispersive X-ray spectrometer (EDXS; JED 2300 EDS). The diameter distribution of the NPLs was determined from equivalent diameters, which accounted for approximately 400 NPLs per sample using Digital Micrograph software.

The magnetic properties of the dried core and hybrid BHF NPLs were measured at room temperature with a vibrating-sample magnetometer (VSM LakeShore 7304, Woburn, MA, USA). Ferrofluids were also measured in the same way, using a special sample holder for liquids. In the case of the liquids, the diamagnetic contribution of the holder and the solvent were first subtracted from the magnetization values obtained
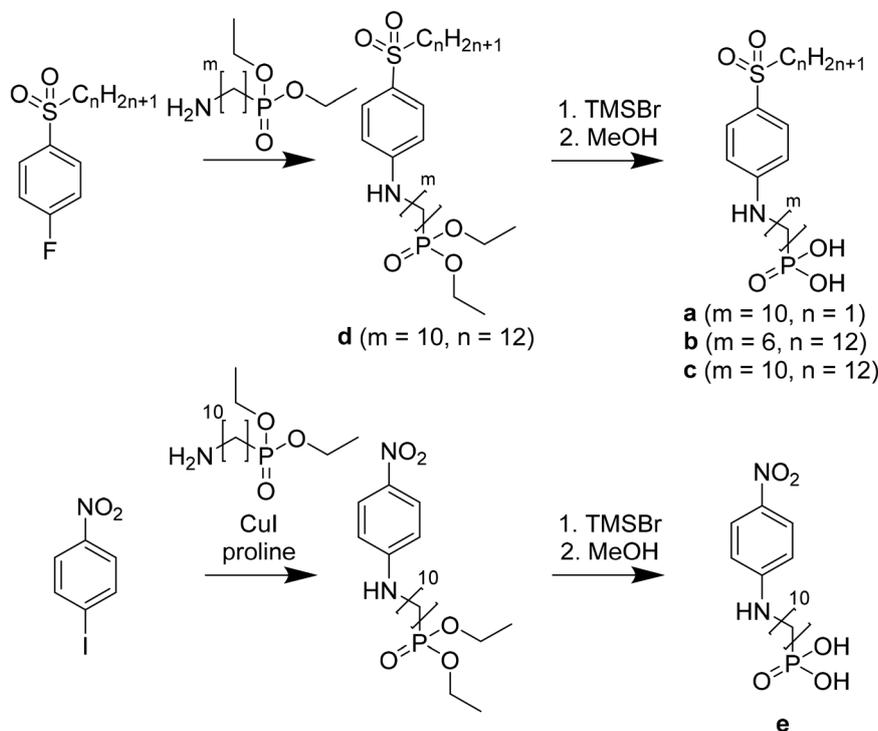
Scheme 2 General protocol for the synthesis of polar ligands.

Table 1 Hybridization conditions for BHF NPLs

Sample	Ligand	Nominal ligand surface density/ molecules per nm^2	Hybridization solvent	Temp./°C
BHF-10**a**-M-50C	a	10	Methanol	50
BHF-3**a**-M-50C	a	3	Methanol	50
BHF-10**a**-H-50C	a	10	1-Hexanol	50
BHF-3**a**-H-50C	a	3	1-Hexanol	50
BHF-3**a**-H-120C	a	3	1-Hexanol	120
BHF-10**b**-M-50C	b	10	Methanol	50
BHF-3**c**-M-50C	c	3	Methanol	50
BHF-10**c**-M-50C	c	10	Methanol	50
BHF-3**c**-H-80C	c	3	1-Hexanol	80
BHF-10**c**-H-80C	c	10	1-Hexanol	80
BHF-10**c**-H-120C	c	10	1-Hexanol	120
BHF-10**c**-H-250C	c	10	1-Hexanol	250
BHF-10**d**-H-120C	d	10	1-Hexanol	120
BHF-3**e**-M-50C	e	3	Methanol	50
BHF-10**e**-M-50C	e	10	Methanol	50
BHF-3**e**-H-80C	e	3	1-Hexanol	80
BHF-10**e**-H-80C	e	10	1-Hexanol	80
BHF-3**e**-H-120C	e	3	1-Hexanol	120

for the ferrofluid. These values are given in Fig. 6 relative to the average measured saturation magnetisation (M_s) value.

Electrokinetic measurements (zeta potential) of the BHF NPLs dispersed in different solvents were measured using a Litesizer 500 (Anton Paar) at a 2 mV potential (corresponding to $E = 0.2$ V m^{-1}) for 500 runs. The reliability of the measurements was precisely controlled (specifically for the suspensions in apolar solvents) by inspecting the phase plot, zeta-potential distribution, and conductivity as presented in more detail in the ESI (Fig. S16† with the description).

The hybridization was also followed using a Fourier-transform infrared (FTIR) spectrometer (Bruker, VERTEX 70/v) with a mono-reflection diamond ATR device (Bruker, A225/Q-DLST) to conduct FTIR measurements. The diamond's refractive index is 2.4. The radiation from the IR source of the spectrometer was focused into the ATR crystal, and the output radiation (from the other side of the crystal) was focused onto an RT-DLa TGS detector. For this purpose, the samples were dried overnight in a dryer at 60 °C. The spectra were acquired in attenuated total reflectance (ATR) mode in the range 4000–100 cm^{-1} with a resolution of 4 cm^{-1}, averaging 128 scans.

Thermogravimetric analyses (TGA) of the pure ligands, core, and hybridized BHF NPLs were carried out using (TGA/DSC2, Mettler Toledo) coupled with a mass spectrometer (OmniStar GSD 350, Pfeiffer Vacuum) for evolved-gas analysis. The samples were heated from 40 to 1100 °C at 20 °C min^{-1} in the flow of synthetic air (20 mL min^{-1}). The number of attached ligand molecules was evaluated from the ligand-decomposition step. Details are given in the ESI.†

The samples' surfaces were analysed using Thin Film Analysis (TFA) XPS spectrometer Physical Electronics Inc. equipped with a monochromatic Al-K X-ray source and a hemispherical electron-energy analyser. XPS survey spectra were acquired to identify elements present on the surface. The high-

energy-resolution spectra of characteristic peaks of the elements Fe 2p, P 2p, S 2p, O 1s, N 1s, and C 1s were recorded over a narrow energy range with a pass energy of 29 eV. The spectra were analysed using MultiPak software package, version 9.9.

Time-of-flight Secondary Ion Mass Spectrometry (ToF SIMS) was measured using a ToF–SIMS 5 instrument (ION-TOF, Münster, Germany) equipped with a bismuth liquid ion gun with a kinetic energy of 30 keV. The SIMS spectra were measured by scanning a Bi_3^+ cluster ion beam over areas from 100×100 μm^2. The dose of primary ions during the measurements was in the static regime. The SIMS spectra were processed with the software SurfaceLab 7.2 (ION TOF). The positive and negative secondary ion mass spectra were measured. The intensities of the SIMS signals were normalized to the total number of emitted secondary ions.

Experimental results

Hybridization of the BHF NPLs with phosphonic ligands

A TEM image of the as-synthesized BHF NPLs is shown in Fig. 2a. Most of the NPLs lie flat on the TEM support while the ones that appear like needles lie (almost) perpendicular to the TEM support. The selected-area diffraction (SAED) confirms the magnetoplumbite structure of the BHF NPLs and all the constituent elements, *i.e.*, Ba, Fe, Sc, and O, were detected with the EDXS. The NPLs have a thickness of approximately 3–5 nm and diameters over a broad range, roughly 10–120 nm (Fig. 2d). The average diameter of the core NPLs was 46 nm with a standard deviation of 21 nm. The thickness and size ranges were similar for all the batches with an average diameter of ~40–50 nm. As expected, no significant change in the morphology and crystal structure of the NPLs was observed after the hybridization (see example in Fig. 2b). The EDXS
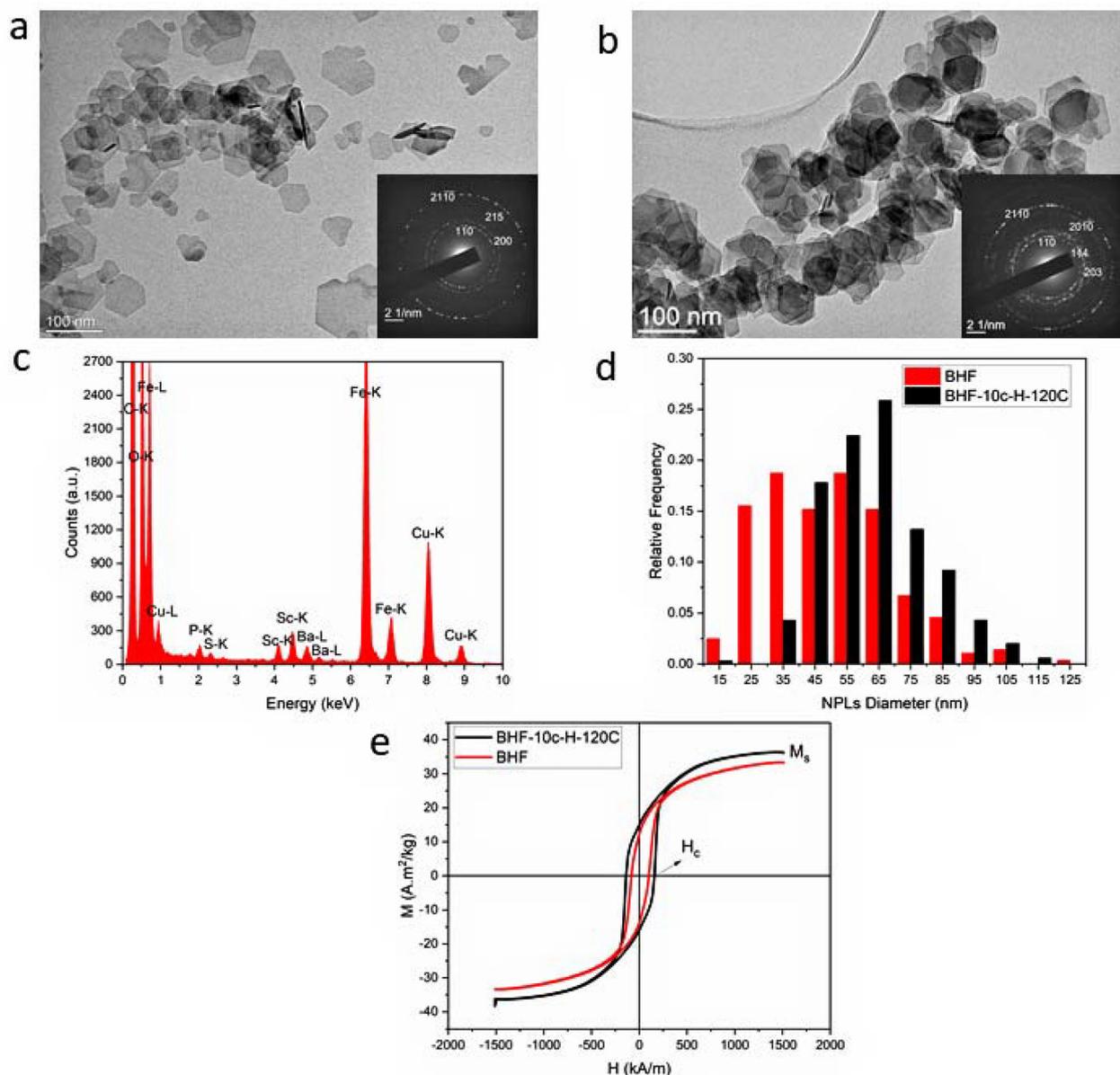
Fig. 2 TEM images with the SAEDs of the BHF NPLs (a) core and (b) BHF-10**c**-H-120C. Indices in the SAEDs correspond to the hexagonal space group $P6_3/mmc$(194). Panel (c) shows the corresponding EDXS spectrum of the hybrid NPLs, panel (d) shows the diameter distributions of the core and hybrid NPLs, and panel (e) shows their magnetic hysteresis loops.

spectrum (Fig. 2c) shows the P and S peaks related to the ligand c along with Ba, Fe, and Sc originating from the BHF. O is present in the NPLs and the ligand, C is present in the ligand, while Cu and C originate from the TEM support grid. Similar results were obtained for all the hybridized BHF NPLs. There was a change in the size distribution and average size (Fig. 2d). The fraction of NPLs with diameters <40 nm was lower for the hybridized NPLs, while their average size was 50 ± 20 nm. The hybridization did not influence the magnetic behaviour of the BHF NPLs (Fig. 2e); they retained their ferrimagnetic character and a magnetic hysteresis with similar coercivity (H_c) values. The small difference between the H_c

values of the two samples could originate from the different size distribution and/or the effect of the samples' packing densities in the VSM holder. In other words, coercivity is an extrinsic property. In contrast, the M_s is an intrinsic property and is reported as the magnetization per mass of a sample. However, due to the presence of non-magnetic species, a direct comparison of the measured M_s values between the samples is not possible. We have to take into account the mass fraction of nonmagnetic phases (*e.g.*, adsorbed CO_2, water, phosphonic ligand) that are present in the samples (Table 2). A detailed analysis is provided in the paragraph discussing Table 2.

Table 2 Fraction of non-magnetic adsorbents and achieved surface density of ligands in the hybrid BHF NPLs with the saturation magnetization (M_s) values of exemplary samples. The "M_s magnetic phase" denotes the calculated M_s value of the BHF NPLs by subtracting the mass of nonmagnetic adsorbents. ΔM_s denotes the relative difference between the M_s magnetic phase of the core and hybridized samples

Sample	Nonmagnetic adsorbents (wt%)	Achieved surface density of a ligand (molecules per nm^2)	M_s measured (Am^2 kg^{-1})	M_s magnetic phase (Am^2 kg^{-1})	ΔM_s (%)
BHF[a]	7.4	0	35.3	38.1	
BHF[b]	7.1	0	33.4	36.0	
BHF[c]	4.7	0	38.5	40.2	
BHF-H-120C[c]*	4.2	0	37.0	38.6	−4.0
BHF-3**a**-M-50C[a]	6.14 ± 0.08	0.3	31.2	36.0	−5.5
BHF-10**a**-M-50C[a]	6.65 ± 0.09	0.3			
BHF-3**a**-H-80C[a]	14.48 ± 0.03	1.5			
BHF-3**a**-H-120C[a]	14.4 ± 0.1	1.5	34.5	40.3	+5.8
BHF-10**c**-H-80C[a]	12.37 ± 0.07	1.5			
BHF-10**c**-H-120C[b]	23.0 ± 0.2	2.1	36.4	45.2	+25
BHF-10**d**-H-120C[b]	7.82 ± 0.04	0.4	39.7	43.1	+20

[a,b,c] denotes the different batches of the core BHF NPLs. * denotes the control sample that was exposed to the hybridization processing conditions in the absence of any ligand.
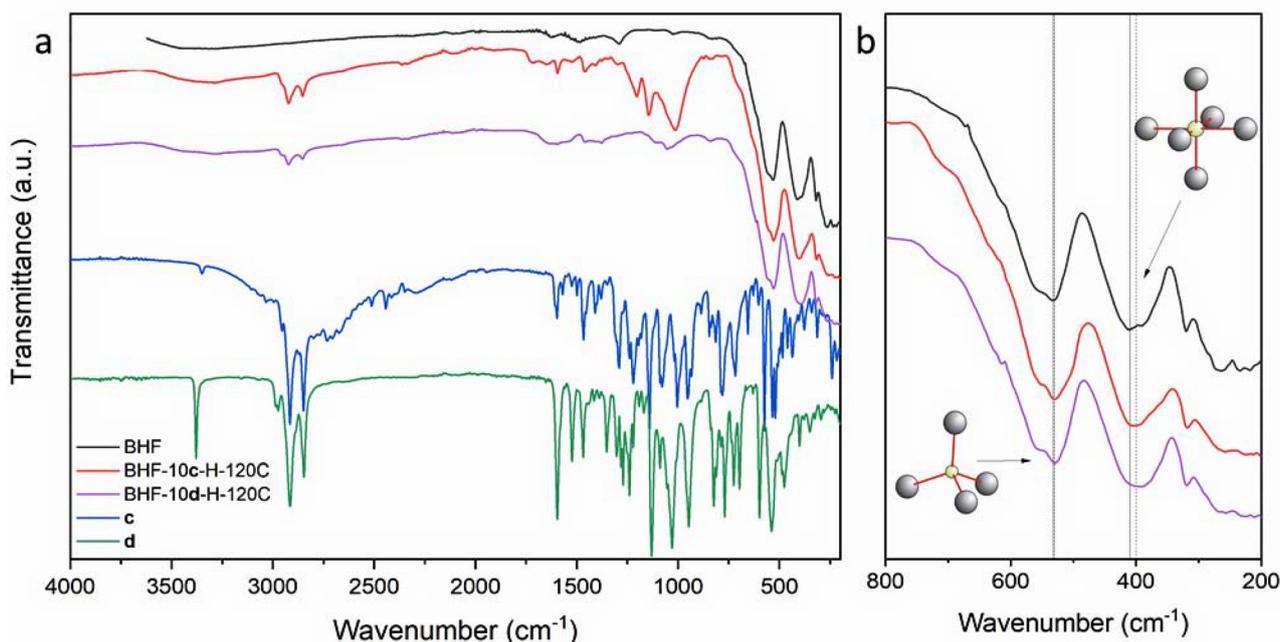

Fig. 3 FTIR spectra of the bare BHF NPLs, BHF-10**c**-H-120C and BHF-10**d**-H-120C and spectra of the pure ligands **c** and **d**. Panels (a) and (b) show different spectral ranges.

FTIR spectra of the bare and selected hybridized BHF NPLs and of the respective pure ligands are shown in Fig. 3. Low-intensity bands that appear at higher wavenumbers can be assigned to the stretching of C=O (1629 cm^{-1}) and N–O (1483 and 1361 cm^{-1}).[49,50] While carbonate is typically adsorbed on powders kept under ambient conditions, the N–O band originates from the nitric acid in the solution with which the BHF NPLs were washed and dispersed after the synthesis. The nitrate ions are counter ions in the aqueous dispersion of positively charged NPLs surfaces. Bare BHF NPLs have only few important bands, all below 800 cm^{-1}. The tetrahedral and octahedral sites of the iron atoms have slightly different vibration energies,[51] which are at 532 and 410 cm^{-1}, respectively in the bare BHF NPLs (Fig. 3b). After the hybridization, we can observe a red shift of approximately 10 cm^{-1}, but only for the band associated with the octahedral coordination of the iron atoms. This indicates that the ligand attached to the surface of the BHF NPLs because the Fe atoms at octahedral positions (*i.e.*, 12k-O) are at the BHF NPLs surfaces.[52] The shift for the octahedral site occurs for both ligands, regardless of the chemical difference between the ligand c being an acid and the ligand d being an ester. At the same time, the N–O

band vanishes suggesting that nitrate ions were removed during the hybridization. Moreover, the NPLs hybridized with the ligand c exhibit multiple vibrations of the phosphonic group in the region from 1400 to 800 cm^{-1}.[53,54] In particular, the band at 1203 cm^{-1} can be assigned to P=O and the band at 873 cm^{-1} can be assigned to P–OH. The bands at 1145 cm^{-1} and 1016 cm^{-1} are related to the asymmetric and symmetric vibrations of the P–O, respectively. These bands do not exclude nor confirm the presence of the P–O–Fe bonds. The FTIR spectra of the other hybrid samples were similar. We can conclude that the phosphonic ligands adsorbed to the BHF NPL surfaces under all the applied conditions (Table 1). However, we could not determine the type of adsorption, *i.e.*, physical or chemical, from the FTIR analysis. Low intensities of the phosphonic vibrations in the case of the BHF-10**d**-H-120C indicate a lower fraction of the attached ligand d in comparison to c (as confirmed with TGA, Table 2). This difference can originate from the different anchor, ester *vs.* acid, respectively.

XPS analyses of the samples were performed to identify the elements present on the surface and to analyse their chemical state. The surface sensitivity of the XPS method is 2–5 nm in depth. The analysis was performed on two different positions for each sample. Fig. 4 shows an XPS survey spectrum of the sample BHF-10**c**-H-120C. The peaks corresponding to Fe 2p, Ba 3d, Sc 2p, and O 1s originate from the BHF NPLs. The additional C 1s peak can be related to the presence of a ligand and/or to surface contamination due to sample exposure to the air before the XPS analyses. Peaks corresponding to S 2p, N 1s, and P 2p were also identified indicating the presence of the ligand c on the surface. Fig. S18 in the ESI† shows a typical high-energy resolution XPS spectra of C 1s, S 2p, P 2p, Sc 2p, and N 1s from the sample BHF-10**c**-H-120C. The main C 1s peak is at 284.4 eV, related to the C atoms in the alkyl chains of the ligand c. In the S 2p spectra the S 2p3/2 peak is observed at 167.8 eV, indicating the S in the 4+ oxidation state from the SO$_2$ groups. The peak P 2p3/2 at 132.8 eV in the P 2p spectra is

related to the PO$_3$ group. The N 1s peak at 399.4 eV is related to the NH group in the ligand. The N 1s peak is partly overlapping with the Sc 2p3/2 and Sc 2p1/2 peaks at 401.1 eV and 405.8 eV, related to the Sc-oxide from the BHF NPLs. In summary, all of the aforementioned groups can be found in the ligand c, which confirms the presence of the ligand in the sample. Similar results can be observed for the sample produced with the same ligand at 50 °C in methanol.

The XPS analyses was complemented with TOF-SIMS to investigate the possible chemisorption of the ligands. The SIMS method has a superior surface sensitivity (2 nm) to the XPS (2–5 nm) and can reveal molecular information from mass spectra of emitted secondary ions from the surface. Among other signals in the SIMS mass spectra, the signals at masses 103 Da and 199 Da were identified as specific to the presence of the ligand c. They are related to the Fe–P–O and the Fe–P–O$_2$ fragments, respectively (Fig. 4b). The two fragments were previously[55] identified as an indication of the chemisorption (*i.e.*, covalent or coordination interaction) of phosphonic acid onto a metal oxide, since they correspond to the Fe–O–P and Fe–O–P–O or O–Fe–O–P bonds, respectively. The maximum relative intensities of the Fe–P–O and Fe–P–O$_2$ signals were measured for the hybrid sample prepared at 120 °C. With an additional increase in the hybridization temperature to 250 °C, the intensity of the Fe–P–O and Fe–P–O$_2$ signals decreases. This can be explained by the onset of the ligand decomposition, starting above 200 °C (Fig. S17†).

The achieved surface densities of ligands in the hybridized BHF NPLs (Table 2) were estimated using TGA and evolved-gas analysis (see details in ESI† with exemplary thermal analyses data Fig. S17†). The ligands' surface densities increased with the hybridization temperature. This coincides with the largest fraction of the chemisorbed fragments detected with TOF-SIMS (Fig. 4b) at 120 °C. The higher the hybridization temperature, the more possible the condensation reaction (Scheme 1). In contrast to this, the physisorbed ligands are in
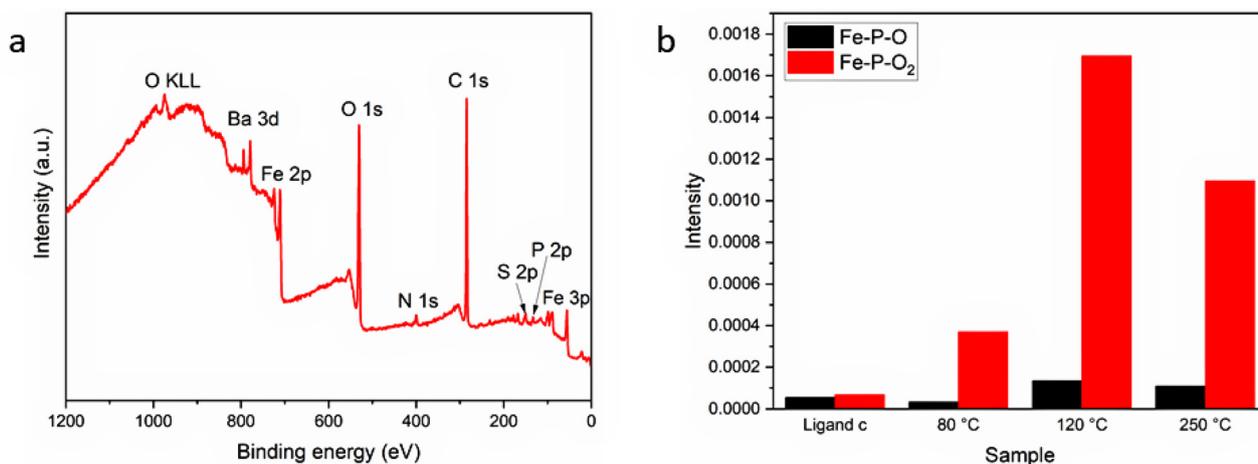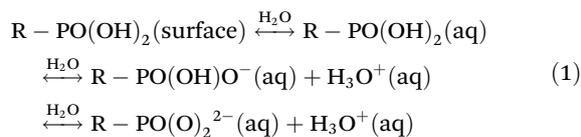

Fig. 4 (a) Survey XPS spectrum of the sample BHF-10**c**-H-120C. (b) TOF-SIMS results for ligand **c**, and the BHF NPLs hybridized with the ligand **c** in 1-hexanol at 80, 120 and 250 °C.

a dynamic equilibrium with the dissolved ligands. The desorption of ligands from a solid surface is promoted in the presence of water.

$$R - PO(OH)_2 (surface) \xrightleftharpoons{H_2O} R - PO(OH)_2 (aq)$$
$$\xrightleftharpoons{H_2O} R - PO(OH)O^- (aq) + H_3O^+ (aq) \qquad (1)$$
$$\xrightleftharpoons{H_2O} R - PO(O)_2{}^{2-} (aq) + H_3O^+ (aq)$$

The adsorption/desorption equilibrium (*i.e.*, the first reaction in eqn (1)) is established in any other solvent solvating the ligands. Consequently, the physisorbed phosphonic ligands can desorb by changing the system's properties, *e.g.*, during dilution or washing.[56] The equilibrium in eqn (1) can also be redirected to the right-hand side in methanol. When compared to 1-hexanol, methanol is more polar and dissolves more water. Consequently, the deprotonation of phosphonic groups and their dissattachment is favoured.

We can also see in Table 2 that the ligands' structure had an effect on the surface density. The ligand c with a longer alkylsulfonyl chain formed a denser assembly when compared to the ligand a. This can be explained by the difference in the polarity with the ligand c being less polar. The lowest surface density was obtained with the ligand d, which is the only ester among the phosphonic acids, *i.e.*, an ester analogue of the ligand c. In this case, the major effect on the different surface densities probably originates in the different anchor.

The room-temperature M_s values of the BHF NPLs increased, *i.e.*, by 5–25%, after they were hybridized in 1-hexanol at 120 °C (Table 2). This was unexpected since the attached ligands are not ferro(i)magnetic and do not contribute to the magnetisation. An increase in the M_s due to the surface phosphonic ligands was measured previously for magnetite nanoparticles[57] and was attributed to the decreased surface spin canting (*i.e.*, origin of the decreased M_s of magnetic nanoparticles *vs.* bulk). The coordinating ligands are supposedly improving the spin alignment of the surface iron ions by minimizing the crystal-structure distortion of the surface *vs.*

the core. Similarly, the M_s values of the spinel ferrite nanoparticles functionalized with carboxyl and catechol moieties increased in comparison to the core nanoparticles. The M_s increase was, in addition to the possibly reduced spin canting, attributed to other reasons,[58–60] such as the redox reaction with catechol stabilizing the surface magnetite layer with a higher M_s than the core maghemite, and an effective increase of the average nanoparticles' size during the processing. In contrast, the adsorbed carboxylates did not improve the surface spin alignment of the core nanoparticles and their M_s was lower.[57] Moreover, an unexpectedly large decrease in the M_s, was obtained in our previous study,[34] in which the BHF NPLs were functionalized with phosphonic acids in an aqueous solution. The M_s decrease was associated with a partial decomposition of the BHF NPLs by di- and tetraphosphonic acids. Since in this study the M_s increased ≥20% in the samples with chemisorbed ligands, we assume that it can be correlated with an improved collinearity of the surface spins.

Ferrofluids from the hybrid BHF NPLs

None of the applied conditions resulted in the maximum-possible surface density of ligands (Table 2), *i.e.*, 3 molecules per nm² (see Calculation section 2). Nevertheless, ~1.5–2 molecules per nm² for the BHF NPLs hybridized at 120 °C with the ligand c was enough to colloidally stabilize the NPLs in 1-hexanol (Fig. 5a). Such surface density seems reasonable, considering the maximum theoretical surface density of 3 phosphonic groups per nm² forming a monolayer at the BHF surface (see Fig. 1). Somewhat higher surface densities from previous studies were correlated with multilayer assemblies of phosphonic acids on metal oxides.[30,34,61] The colloidal stability in 1-hexanol was obtained with 4–5-times lower surface density of the ester ligand d (Table 2). This indicates that the condensation reaction (similar to Scheme 1 but with ethanol as a side product) took place at 120 °C also with the ester anchor. Stable ferrofluids were also obtained after hybridizing
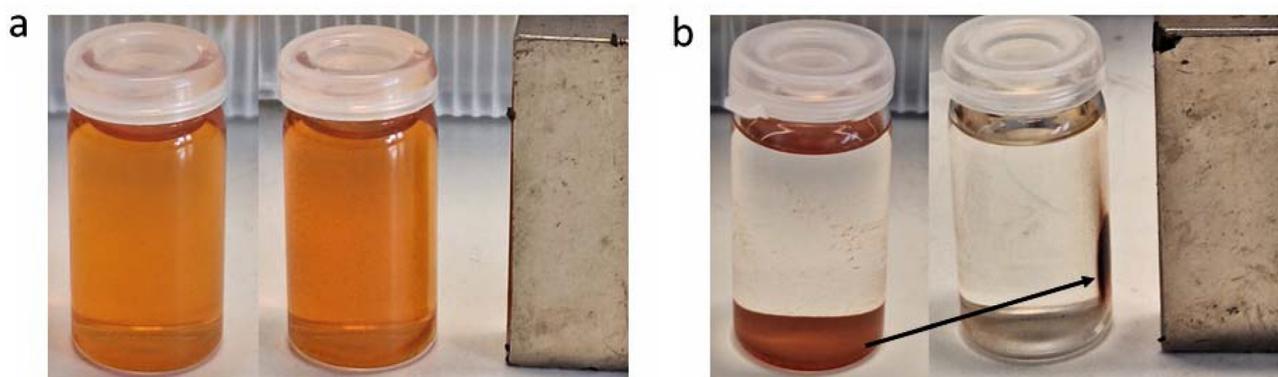

Fig. 5 Photographs of the dispersions of: (a) BHF-10**c**-H-120C (b) BHF-10**c**-H-80C. The difference between the stable ferrofluids and unstable systems under an applied magnetic field is shown in the images (a) and (b), respectively. While the NPLs in a stable ferrofluid (a) remain dispersed also in a magnetic field induced by a permanent magnet, the NPLs in the unstable system (b) sediment (left photograph) and the sediment is attracted by a magnet (right photograph).

Table 3 Colloidal properties of the hybridized BHF NPLs dispersed in different solvents. The dielectric constants increase from 2.27 to 2.38, 13.3 and 32.7 for *p*-xylene to toluene, 1-hexanol and methanol, respectively[62,69–71]

Sample	Dispersing solvent	Zeta potential (mV)	Conductivity ($\mu S\ cm^{-1}$)	Colloidal stability
BHF	Methanol	-15.0 ± 0.2	8	No
BHF-10**a**-M-50C	Methanol	-44.0 ± 0.2	11	No
	1-Hexanol	0	0	No
	Toluene	0	0	No
BHF-3**a**-H-50C	1-Hexanol	0	0	No
BHF-3**a**-H-120C	1-Hexanol	0	0	Yes
BHF-10**b**-M-50C	Methanol	-50.0 ± 0.7	28	No
	Xylene	0	0	No
BHF-3**c**-M-50C	Methanol	-44.7 ± 1.3	17	No
BHF-10**c**-M-50C	Methanol	-47.6 ± 0.6	10	No
BHF-3**c**-H-80C	1-Hexanol	0	0	No
BHF-10**c**-H-80C	1-Hexanol	0	0	No
BHF-10**c**-H-120C	1-Hexanol	0	16	Yes
BHF-10**d**-H-120C	1-Hexanol	0	0	Yes
BHF-3**e**-H-120C	1-Hexanol	0	0	Yes

the NPLs at 120 °C with the ligands a and e, the latter has a nitro ending group and the largest dipole moment (Chart 1). We conclude that the ferrofluids from BHF NPLs in 1-hexanol can be obtained by hybridizing the BHF NPLs with polar phosphonic ligands at an approximate surface density of 0.5 molecules per nm² or higher.

All dispersions of the hybridized NPLs in 1-hexanol had zero zeta-potential (Table 3), indicating a monolayer assembly of the ligands (Fig. S19a†). Due to the relatively low polarity (*i.e.*, dielectric constant of 1-hexanol is 13.3[62]), the phosphonic acid remains protonated and cannot introduce any surface charge, regardless of the bonding interaction. Accordingly, zero conductivity was measured due to a negligible ionic strength. The same is valid for the dispersions in less polar solvents, *i.e.*, xylene and toluene. However, they were not colloidally stable. This coincides with negligible solubility and a lack of solvation of the ligands in the two nonpolar solvents.

The zeta-potential of the hybrid NPLs in methanol was between −22 and −50 mV, more negative than that of the core BHF NPLs, *i.e.*, −15 mV (Table 3). This indicates an attachment of the polar ligands on the NPL surfaces in methanol. The more negative zeta-potential values of the dispersed hybrid NPLs are attributed to the higher density of negatively charged species on the NPL surfaces in comparison to the core NPLs. The only negatively charged species in the reaction system, besides the possibly deprotonated surface hydroxyl groups (crystal–Fe–O⁻), are phosphonic groups of the polar ligands (Chart 1). The remaining unbound P–OH group (Scheme 1) at the very surface can deprotonate in methanol and with it, the zeta-potential becomes more negative than for the core NPLs. Such dissociated P–O– groups at the very surface are repelled from the dissociated surface sites of the core NPLs (crystal–Fe–O–). Consequently, the surface density of the ligands in methanol should be low, which, indeed, was true (Table 2). The question is whether methanol is sufficiently polar or if it contains a sufficient concentration of water to enable the deprotonation of the second P–OH group.

Alternatively, an increase in the negative surface charge can arise from a bilayer at the BHF NPL surface (Fig. S19b and c in

ESI†). The bilayer formation is driven by the hydrophobic and/ or π–π interaction between the adsorbed and desorbed amphiphilic ligands in a polar solvent. In the second layer, free P–OH groups can deprotonate in methanol, thus, increasing the negative surface charge. The association of the deprotonated ligands in methanol can occur before the adsorption of ligands on the surface, and the ligands adsorb as associates. Due to the steric hindrances of the primary adsorbed associates, the adsorption of additional associates on the surface is limited, which explains the low surface densities of the ligands (Table 2). The ligands' deprotonation results in an increased ionic strength, as was confirmed by the relatively high conductivity of the methanol dispersions (Table 3). The large ionic strength explains the colloidal instability of the methanol systems despite the relatively large absolute values of the zeta-potential.
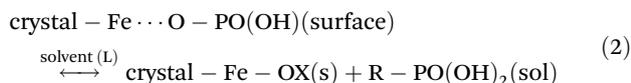
All the hybridized BHF NPLs with nominal surface densities of 3 and 10 molecules per nm² have roughly similar zeta-potentials in methanol, suggesting a similar density of the surface charge and, consequently, a similar density of the attached ligands, as also evident from the TGA results (Table 2). This result implies that the excessive unbound ligands from the samples with nominal 10 molecules per nm² are removed to a large extent during the washing step, while the bonded ligands are physisorbed, possibly *via* a hydrogen bond, *i.e.*, in plain adsorption mode (Fig. 1). The calculations (section 2) suggest inferior stability of the plain adsorption in comparison to the adsorption *via* condensation (*i.e.*, chemisorption), which is in accordance with our experimental observation.
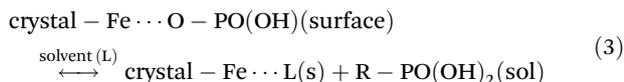
Discussion

Our study shows that a stable hybridization is possible between the surfaces of BHF NPLs and phosphonic acids (Chart 1). A significant fraction of the fragments Fe–P–O and Fe–P–O₂ (Fig. 4b) indicates chemisorption,[55] *i.e.*, a covalent or

coordination interaction between the surface iron ions and the phosphonic moiety. Similar to what was reported previously,[39,55] the chemisorption was promoted using an excessive ligand fraction at elevated temperatures, with the highest efficiency being at 120 °C. The higher temperature promotes the condensation reaction (Scheme 1) when the evaporation of water directs the equation to the right-hand side. If the condensation results in a covalent interaction between the ligands and the surface, the attachment is irreversible. However, the ligands could also chemisorb onto the BHF NPL surfaces *via* a coordination interaction that competes with the interaction ligand–solvent and metal–oxide surface–solvent.

$$
\begin{aligned}
&\text{crystal} - \text{Fe} \cdots \text{O} - \text{PO(OH)(surface)} \\
&\xleftrightarrow{\text{solvent (L)}} \text{crystal} - \text{Fe} - \text{OX(s)} + \text{R} - \text{PO(OH)}_2(\text{sol})
\end{aligned}
\quad (2)
$$

Here, X denotes the surface reconstruction in a solvent. If the solvent is water or alcohol, X = H. The phosphonic ligands can also exchange for the solvent molecules (L) if the solvation interaction is stronger than the coordination with the surface.

$$
\begin{aligned}
&\text{crystal} - \text{Fe} \cdots \text{O} - \text{PO(OH)(surface)} \\
&\xleftrightarrow{\text{solvent (L)}} \text{crystal} - \text{Fe} \cdots \text{L(s)} + \text{R} - \text{PO(OH)}_2(\text{sol})
\end{aligned}
\quad (3)
$$

Water molecules strongly interact (*i.e.*, hydration) with the phosphonic moieties, especially at the pH values at which the phosphonic moiety deprotonates and the phosphonic ligand at the surface can be exchanged for a proton (eqn (2)).[63,64] Water molecules can also exchange the coordination ligands if the hydration interaction is dominant (eqn (3)). A complete miscibility of methanol with water shifts the reaction in Scheme 1 to the left-hand side and the high polarity of methanol promotes the deprotonation and association of ligands (Fig. S19b and c†), resulting in a negative effect on their surface density (Table 2). Therefore, the primarily selected solvent in our study, *i.e.*, methanol, was not suitable for hybridizing the BHF NPLs with phosphonic ligands. Instead, we selected 1-hexanol, which is immiscible with water (Fig. S15†), has sufficiently low polarity for stabilizing the protonated form of the phosphonic ligands and sufficiently high boiling point (157 °C) for the high-temperature hybridization process. Our findings are in line with previous research[65] suggesting the promotion of denser and more stable phosphonic monolayers by low dielectric solvents.

We performed an experiment to examine whether the chemisorbed phosphonic-BHF hybrids are stable against water (eqn (3)) and protons (eqn (2)). An aqueous nitric acid solution (pH 2) was added to the 1-hexanol ferrofluid of BHF-10**c**-H-120C. The two phases do not mix simultaneously. The lower density 1-hexanol phase stays on the top and is coloured due to the dispersed NPLs. After a vigorous stirring of the two phases together for 24 h, they separated in the same manner as before the stirring (Fig. S20†). We conclude that the ligands attached to the BHF NPLs in 1-hexanol at 120 °C do not exchange by protons nor water molecules.

An additional experiment was carried out to verify the stability of the ligands' attachment to the NPLs against methanol, in which the ligands are fully soluble. The hybridized NPLs transferred from 1-hexanol to methanol have negative zeta-potential values of around −25 to −30 mV. The absolute values of the zeta-potential are higher than for the core BHF NPLs but 20–45% lower than for the NPLs hybridized in methanol (Table 3), implying the reassembly of the ligands' molecules into bilayers (Fig. S19b and c†). To form a bilayer, a part of the molecules should desorb from the surface, which can be expected for the physisorbed ligands (eqn (1)). However, the negative zeta-potential in methanol was also measured for the hybrids with chemisorbed ligands obtained at 120 °C in 1-hexanol. There are several explanations: (i) a fraction of the ligand's molecules is not chemisorbed but physisorbed, they desorb in methanol and form a bilayer, (ii) deprotonation of the unbound P–OH group at the very surface (see Fig. S19†), or (iii) the ligands are coordinated (*i.e.*, not covalently bonded) to the NPL surface but the solvation interaction with the methanol molecules is stronger, leading to an equilibrium between the adsorbed and desorbed ligands (eqn (3)). The latter dissolve in methanol but can form a dynamic bilayer assembly driven by the hydrophobic or π–π interactions (Fig. S19b and c†).

An increase in the M_s values after hybridizing the BHF NPLs with phosphonic ligands (Table 2) can be explained by a reduction of the surface spin canting, similar to ref. 57. Remember that the M_s increase was measured only for the NPLs hybridized at 120 °C, onto which the ligands chemisorbed. But let us first comment on a possible positive effect of size on the M_s. Since the M_s of nanoparticles decreases with the decreasing size due to the increased surface spin canting,[66] we compared the diameter-size distributions of the core and functionalized NPLs (Fig. 2d). The M_s values of the BHF NPLs are mostly affected by the variation in their thicknesses due to the relatively large *c*-unit-cell parameter (~2.5 nm) whereas the diameter is associated with much smaller (~0.6 nm) *a* and *b* parameters. Most of the NPLs with diameters of 30–300 nm have thicknesses of 4.1 nm and their M_s values are not significantly affected by the diameter distribution.[67] The measured M_s of the sample containing mostly the BHF NPLs with diameters ≤30 nm was ~25 Am^2 kg^{-1}.[48] Around 20% of the core BHF NPLs from this study have diameters between 15 and 30 nm (Fig. 2d). If these 20% of NPLs would be wider than 30 nm, the M_s of the core BHF NPLs would be ~39 Am^2 kg^{-1} and the increase of the M_s would still be significant, *i.e.*, ~13 and ~10% for the BHF-10**c**-H-120C and BHF-10**d**-H-120C, respectively. Therefore, there also has to be a contribution from the changed surface chemistry to the measured increase in the M_s. As a proof, we conducted a control experiment. The BHF NPLs were exposed to the hybridizing process but without any ligand, the sample BHF-H-120C. A 4% decrease of the M_s was measured, similar to that for the BHF-3**a**-M-50C with the physisorbed ligand. We conclude that chemisorbing the phosphonic ligands onto the BHF NPLs improves the spin collinearity at the surface and,

with it, their M_s increases. Different experimental observations from various studies (*e.g.*, in ref. 57–60) showing an increase/decrease of the M_s of magnetic nanoparticles after their functionalization originate from different attachment modes that depend on the composition of the magnetic nanoparticles and the ligand, as well as the processing parameters.

Although we cannot conclude whether the covalent interaction is possible in the studied system, we improved the stability of the attached phosphonic ligands in comparison to previous studies[63,64] by using 1-hexanol instead of water and temperature above the boiling point of water during our hybridization process. A stable hybrid sample was also prepared using an ester ligand d that cannot deprotonate and induce the surface exchange of the phosphonic ligand with a proton. Its surface density was ~4–5 times lower than that of the phosphonic acids, which may be due to the different mechanism involving hydrolysis of an ester group prior to the condensation or release of ethanol instead of water during the condensation (Scheme 1).[40,68] The hydrolysis of phosphonic esters is catalysed by acids or bases and also by metal ions, *e.g.*, on metal oxide surfaces. The latter reason, in combination with the heating to 120 °C, speaks in favour of the two-step mechanism for attachment of the phosphonic ester to the BHF NPLs. The additional step can reduce the rate of condensation when compared to phosphonic acids. This explains the lower surface density of ligand d. Regardless of this, a stable ferrofluid was obtained in 1-hexanol from the BHF-10**d**-H-120C NPLs.

It seems that the solvation of the chemisorbed ligand layer in 1-hexanol directed the assembly of the ligands towards a short-range electrostatic repulsion (Fig. 6a), which suppressed the agglomeration of the NPLs in combination with the steric repulsion. The range of this dipolar electrostatic repulsion is estimated to be of the order of the thickness of the hybrid, *i.e.*, 5–10 nm, which is comparable to the Debye length in the electrostatically stabilized suspensions.[11] Roughly 1.5–2 molecules per nm^2 of chemisorbed phosphonic ligands a and c, and only ~0.5 molecules per nm^2 of the ligand d (Tables 2 and 3) efficiently stabilized the BHF NPLs in 1-hexanol. Lack of the magnetic interaction between the hybrid NPLs in 1-hexanol results in a superparamagnetic behaviour of the ferrofluids (Fig. 6b). The ferrofluids show no remanent magnetization but they are responsive to a low magnetic field of around 10–20 kA m^{-1} (Fig. 6b). The combination of the high sensitivity to a magnetic field with their NPLs specific shape and uniaxial magnetocrystalline anisotropy results in a strong magneto-optic effect (Movie S1 in ESI†). The hybrid BHF NPLs align with their basal planes perpendicular to the direction of an applied magnetic field and, consequently, rotate with the rotating magnet, showing a birefringence. The new ferrofluids from permanently magnetic BHF NPLs in 1-hexanol do not conduct electric current (Table 3). They can substitute for the conductive BHF ferrofluids in 1-butanol,[10,13] enabling sensor applications in an electric field without an electrical breakdown.
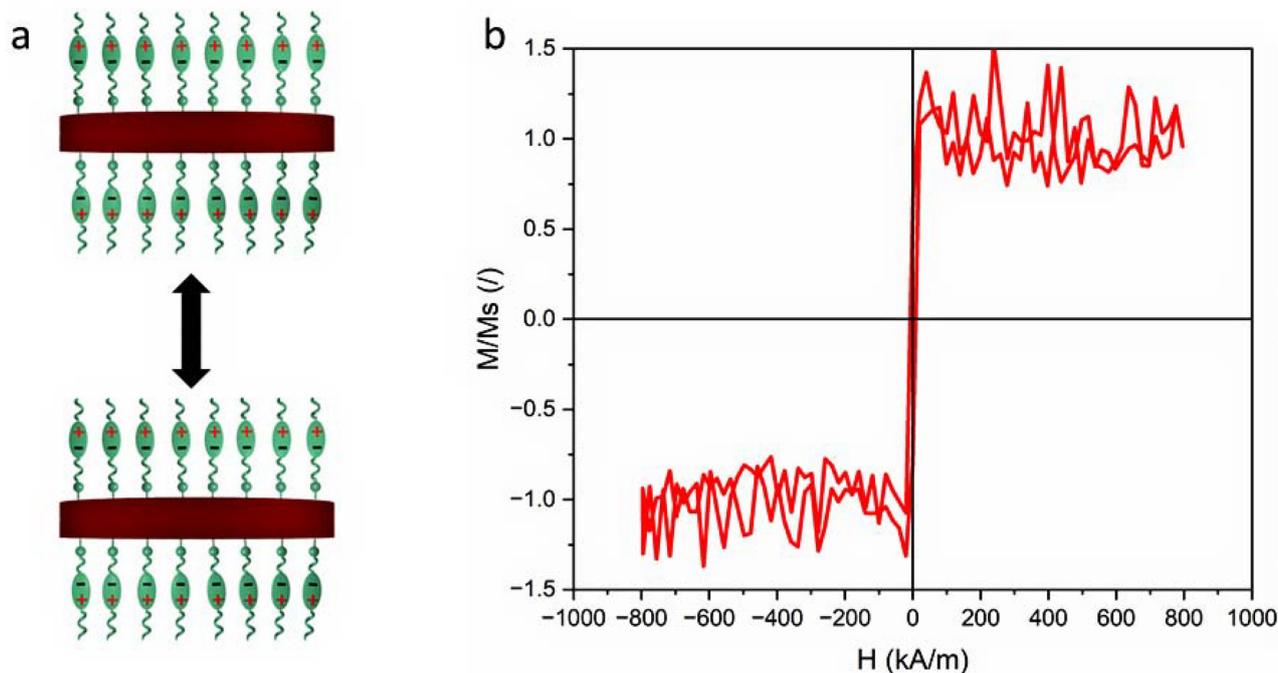

Fig. 6 Ferrofluid of the BHF NPLs hybridized with phosphonic ligands in a low-polar solvent: (a) schematic of two approaching hybrid NPLs. The NPLs align in *via* the magnetic dipolar interaction that is surpassed by the electrostatic dipolar repulsive interaction. (b) Superparamagnetic behaviour of the ferrofluid from BHF-10**c**-H-120C NPLs (0.1 mg mL^{-1}).

Conclusions

We prepared the first stable dispersions of permanently magnetic BHF NPLs (with $M_s \sim$ 40–45 $Am^2\ kg^{-1}$) in a solvent of intermediate polarity, in which the NPLs were stabilized when hybridized with polar phosphonic ligands. The synthesized polar ligands had calculated dipole moments between 7.53 and 8.88 D. The stable colloids were obtained only when the polar ligands chemisorbed on the surfaces of BHF NPLs with a minimum surface density of around 0.5 molecules per nm^2. This means that a robust attachment of the ligands on at least 15% of the available surface sites ensures a sufficient steric-solvation repulsion for minimizing the magnetic dipolar attraction between the BHF NPLs in 1-hexanol. The new colloids of permanently magnetic BHF NPLs in 1-hexanol can be exploited for the development of novel magneto-optic sensors.

Other important findings from the study are relevant for understanding the hybridization of metal oxide surfaces with polar phosphonic acids and applications of the new systems:

1. Chemisorption of phosphonic ligands to a metal oxide surface is only possible at a sufficiently high temperature, $e.g.$, 120 °C for iron oxides, in an anhydrous solvent, favouring the condensation reaction.

2. At low temperatures and in water or water-miscible solvents, physisorption is favoured against chemisorption, resulting in a low surface density of adsorbed ligands and colloidal instability.

3. If the phosphonic group of a ligand deprotonates in a solvent, the ligands can desorb and assemble in bilayers at the metal oxide surfaces. Such dispersions have poor or no colloidal stability in the respective solvent.

4. BHF NPLs are colloidally stable in a solvent of intermediate-to-low polarity when hybridized with fully protonated polar phosphonic ligands at surface densities of ≥0.5 molecules per nm^2.

5. The dominating stabilizing colloidal interaction is electrostatic dipolar repulsion induced by solvation interaction between the surface ligand and solvent molecules. The same approach is suitable for hybridizing and colloidally stabilizing any other metal oxide nanoparticles.

6. By tuning the polarity of the phosphonic push-pull systems or by coupling them with nonpolar molecules, stable dispersions of BHF NPLs in apolar solvents can be obtained in the future.

7. Saturation magnetisation of the BHF NPLs increased after the hybridization by suppressing the surface spin canting. In other words, the hybrid BHF NPLs have superior sensitivity to a magnetic field than the core NPL. Consequently, magneto-optic sensors based on the ferrofluid from hybrid BHF NPLs will operate at lower NPL concentrations (order of 0.1 mg mL^{-1}) than those based on the core NPLs ($e.g.$, >1 mg mL^{-1} (ref. 10)).

8. The obtained dispersions in 1-hexanol have negligible conductivity and can be used in applications in an electric field.

Author contributions

Data availability

The data for this article, including raw data of magnetic, spectroscopic, HPLC, and TGA measurements will be available at **https://zenodo.org/records/15100328** upon publishing.

Conflicts of interest

There are no conflicts to declare.

Acknowledgements

References

1   J. M. Ginder, Behavior of magnetorheological fluids, *MRS Bull.*, 1998, **23**(8), 26–29.
2   J. De Vicente, D. J. Klingenberg and R. Hidalgo-Alvarez, Magnetorheological fluids: a review, *Soft Matter*, 2011, 7(8), 3701–3710.
3   S. Genc and B. Derin, Synthesis and rheology of ferrofluids: a review, *Curr. Opin. Chem. Eng.*, 2014, **3**, 118–124.

4 M. Kole and S. Khandekar, Engineering applications of ferrofluids: A review, *J. Magn. Magn. Mater.*, 2021, **537**, 168222.

5 S. Ovtar, D. Lisjak and M. Drofenik, Barium hexaferrite suspensions for electrophoretic deposition, *J. Colloid Interface Sci.*, 2009, **337**(2), 456–463.

6 M. Shuai, A. Klittnick, Y. Shen, G. P. Smith, M. R. Tuchband, C. Zhu, *et al.*, Spontaneous liquid crystal and ferromagnetic ordering of colloidal magnetic nanoplates, *Nat. Commun.*, 2016, **7**(1), 10394.

7 Ž Gregorin, N. Sebastián, N. Osterman, P. H. Boštjančič, D. Lisjak and A. Mertelj, Dynamics of domain formation in a ferromagnetic fluid, *J. Mol. Liq.*, 2022, **366**, 120308.

8 T. Goršak, D. Makovec, U. Javornik, B. Belec, S. Kralj and D. Lisjak, A functionalization strategy for the dispersion of permanently magnetic barium-hexaferrite nanoplatelets in complex biological media, *Colloids Surf., A*, 2019, **573**, 119–127.

9 A. A. Eliseev, L. A. Trusov, E. O. Anokhin, A. P. Chumakov, V. V. Korolev, A. E. Sleptsova, *et al.*, Tunable order in colloids of hard magnetic hexaferrite nanoplatelets, *Nano Res.*, 2022, **15**, 898–906.

10 V. Budinski, S. Pevec, S. Čampelj, A. Mertelj, D. Lisjak and D. Donlagic, Miniature magneto-optic angular position sensor, *Opt. Lett.*, 2022, **47**(18), 4696–4699.

11 P. Medle Rupnik, D. Lisjak, M. Čopič and A. Mertelj, Ferromagnetic liquid crystals for magnetic field visualisation, *Liq. Cryst.*, 2015, **42**(12), 1684–1688.

12 P. Medle Rupnik, D. Lisjak, M. Čopič, S. Čopar and A. Mertelj, Field-controlled structures in ferromagnetic cholesteric liquid crystals, *Sci. Adv.*, 2017, **3**(10), e1701336.

13 P. Hribar Boštjančič, M. Tomšič, A. Jamnik, D. Lisjak and A. Mertelj, Electrostatic Interactions between Barium Hexaferrite Nanoplatelets in Alcohol Suspensions, *J. Phys. Chem. C*, 2019, **123**(37), 23272–23279.

14 J. N. Israelachvili, *Intermolecular and surface forces*, Academic press, 2011.

15 R. Müller, R. Hiergeist, W. Gawalek, A. Hoell and A. Wiedenmann, Magnetic and structural investigations on barium hexaferrite ferrofluids, *J. Magn. Magn. Mater.*, 2002, **252**, 43–45.

16 R. Müller, R. Hergt, S. Dutz, M. Zeisberger and W. Gawalek, Nanocrystalline iron oxide and Ba ferrite particles in the superparamagnetism–ferromagnetism transition range with ferrofluid applications, *J. Phys.: Condens. Matter*, 2006, **18**(38), S2527.

17 N. Gautam and R. Singh, Magneto-viscosity of stable colloidal solutions of Barium-strontium hexaferrite ferrofluid, *Mater. Res. Express*, 2019, **6**(8), 084012.

18 N. Gautam, G. Thirupathi and R. Singh, Magnetoviscosity of paraffin-based barium ferrite ferrofluid, *IEEE Trans. Magn.*, 2016, **52**(7), 1–4.

19 P. H. Boštjančič, *Mechanisms for colloidal stabilization of magnetic nanoplatelets*, Institute Jozef Stefan, Ljubljana, 2022.

20 J. C. Love, L. A. Estroff, J. K. Kriebel, R. G. Nuzzo and G. M. Whitesides, Self-Assembled Monolayers of Thiolates on Metals as a Form of Nanotechnology, *Chem. Rev.*, 2005, **105**(4), 1103–1170.

21 L. Feng, S. Li, Y. Li, H. Li, L. Zhang, J. Zhai, *et al.*, Super–hydrophobic surfaces: from natural to artificial, *Adv. Mater.*, 2002, **14**(24), 1857–1860.

22 G. Guerrero, J. G. Alauzun, M. Granier, D. Laurencin and P. H. Mutin, Phosphonate coupling molecules for the control of surface/interface properties and the synthesis of nanomaterials, *Dalton Trans.*, 2013, **42**(35), 12569–12585.

23 S. P. Pujari, L. Scheres, A. T. Marcelis and H. Zuilhof, Covalent surface modification of oxide surfaces, *Angew. Chem., Int. Ed.*, 2014, **53**(25), 6322–6356.

24 I. V. Chernyshova, S. Ponnurangam and P. Somasundaran, Adsorption of Fatty Acids on Iron (Hydr)oxides from Aqueous Solutions, *Langmuir*, 2011, **27**(16), 10007–10018.

25 F. Schwarz, S. Pomp, P. Seidel, X. Li, J. Paier and M. Sterrer, Hydrogen-bond-stabilized high density catechol monolayer on magnetite Fe_3O_4 (111), *Surf. Sci.*, 2022, **719**, 122027.

26 H.-Y. Nie, M. J. Walzak and N. S. McIntyre, Delivering octadecylphosphonic acid self-assembled monolayers on a Si wafer and other oxide surfaces, *J. Phys. Chem. B*, 2006, **110**(42), 21101–21108.

27 L. Zeininger, L. Portilla, M. Halik and A. Hirsch, Quantitative determination and comparison of the surface binding of phosphonic acid, carboxylic acid, and catechol ligands on TiO_2 nanoparticles, *Chem. – Eur. J.*, 2016, **22**(38), 13506–13512.

28 P. J. Hotchkiss, S. C. Jones, S. A. Paniagua, A. Sharma, B. Kippelen, N. R. Armstrong, *et al.*, The modification of indium tin oxide with phosphonic acids: mechanism of binding, tuning of surface properties, and potential for use in organic electronic applications, *Acc. Chem. Res.*, 2012, **45**(3), 337–346.

29 L. Portilla, S. H. Etschel, R. R. Tykwinski and M. Halik, Green Processing of Metal Oxide Core–Shell Nanoparticles as Low–Temperature Dielectrics in Organic Thin–Film Transistors, *Adv. Mater.*, 2015, **27**(39), 5950–5954.

30 W. Gao, L. Dickinson, C. Grozinger, F. G. Morin and L. Reven, Self-assembled monolayers of alkylphosphonic acids on metal oxides, *Langmuir*, 1996, **12**(26), 6429–6435.

31 C. Queffelec, M. Petit, P. Janvier, D. A. Knight and B. Bujoli, Surface modification using phosphonic acids and esters, *Chem. Rev.*, 2012, **112**(7), 3777–3807.

32 D.-H. Xia, C. Pan, Z. Qin, B. Fan, S. Song, W. Jin, *et al.*, Covalent surface modification of LY12 aluminum alloy surface by self-assembly dodecyl phosphate film towards corrosion protection, *Prog. Org. Coat.*, 2020, **143**, 105638.

33 F. Brodard-Severac, G. Guerrero, J. Maquet, P. Florian, C. Gervais and P. H. Mutin, High-field 17O MAS NMR investigation of phosphonic acid monolayers on titania, *Chem. Mater.*, 2008, **20**(16), 5191–5196.

34 D. Lisjak, P. Hribar Boštjančič, A. Mertelj, A. Mavrič, M. Valant, J. Kovač, *et al.*, Formation of Fe(III)-phosphonate coatings on barium hexaferrite nanoplatelets for porous nanomagnets, *ACS Omega*, 2020, **5**(23), 14086–14095.

35 H. Ma, O. Acton, D. O. Hutchins, N. Cernetic and A. K.-Y. Jen, Multifunctional phosphonic acid self-assembled monolayers on metal oxides as dielectrics, interface modification layers and semiconductors for low-voltage high-performance organic field-effect transistors, *Phys. Chem. Chem. Phys.*, 2012, **14**(41), 14110–14126.

36 C. S. Pauly, A.-C. Genix, J. G. Alauzun, M. Sztucki, J. Oberdisse and P. H. Mutin, Surface modification of alumina-coated silica nanoparticles in aqueous sols with phosphonic acids and impact on nanoparticle interactions, *Phys. Chem. Chem. Phys.*, 2015, **17**(29), 19173–19182.

37 G. Guerrero, P. H. Mutin and A. Vioux, Organically modified aluminas by grafting and sol–gel processes involving phosphonate derivatives, *J. Mater. Chem.*, 2001, **11**(12), 3161–3165.

38 L. Zeininger, L. M. Stiegler, L. Portilla, M. Halik and A. Hirsch, Manufacturing nanoparticles with orthogonally adjustable dispersibility in hydrocarbons, fluorocarbons, and water, *ChemistryOpen*, 2018, **7**(4), 282–287.

39 P. H. Mutin, G. Guerrero and A. Vioux, Hybrid materials from organophosphorus coupling molecules, *J. Mater. Chem.*, 2005, **15**(35–36), 3761–3768.

40 G. Guerrero, P. Mutin and A. Vioux, Anchoring of phosphonate and phosphinate coupling molecules on titania particles, *Chem. Mater.*, 2001, **13**(11), 4367–4373.

41 M. J. Frisch, G. W. Trucks, H. B. Schlegel, G. E. Scuseria, M. A. Robb and J. R. Cheeseman, *et al.*, *Gaussian 16 Rev. C.01*, Wallingford, CT, 2016.

42 J. P. Perdew, K. Burke and M. Ernzerhof, Generalized gradient approximation made simple, *Phys. Rev. Lett.*, 1996, **77**(18), 3865.

43 F. Weigend, Accurate Coulomb-fitting basis sets for H to Rn, *Phys. Chem. Chem. Phys.*, 2006, **8**(9), 1057–1065.

44 D. Lisjak, I. Arčon, M. Poberžnik, G. Herrero-Saboya, A. Tufani, A. Mavrič, *et al.*, Saturation magnetisation as an indicator of the disintegration of barium hexaferrite nanoplatelets during the surface functionalisation, *Sci. Rep.*, 2023, **13**(1), 1092.

45 M. Poberžnik, G. Herrero-Saboya, D. Makovec, D. Lisjak and L. Martin-Samos, Surface phase diagrams of pristine and hydroxylated barium hexaferrite surfaces from first-principles atomistic thermodynamics, *Appl. Surf. Sci.*, 2023, **637**, 157890.

46 P. Gilli, V. Bertolasi, L. Pretto, V. Ferretti and G. Gilli, Covalent versus electrostatic nature of the strong hydrogen bond: discrimination among single, double, and asymmetric single-well hydrogen bonds by variable-temperature X-ray crystallographic methods in β-diketone enol RAHB systems, *J. Am. Chem. Soc.*, 2004, **126**(12), 3845–3855.

47 S. Ramachandran, B.-L. Tsai, M. Blanco, H. Chen, Y. Tang and W. A. Goddard, Self-assembled monolayer mechanism for corrosion inhibition of iron by imidazolines, *Langmuir*, 1996, **12**(26), 6419–6428.

48 D. Lisjak and M. Drofenik, Chemical Substitution—An Alternative Strategy for Controlling the Particle Size of Barium Ferrite, *Cryst. Growth Des.*, 2012, **12**(11), 5174–5179.

49 I. E. Wachs, Infrared spectroscopy of supported metal oxide catalysts, *Colloids Surf., A*, 1995, **105**(1), 143–149.

50 K. I. Hadjiivanov, Identification of neutral and charged N x O y surface species by IR spectroscopy, *Catal. Rev.*, 2000, **42**(1–2), 71–144.

51 K. Bamzai, G. Kour, B. Kaur, M. Arora and R. Pant, Infrared spectroscopic and electron paramagnetic resonance studies on Dy substituted magnesium ferrite, *J. Magn. Magn. Mater.*, 2013, **345**, 255–260.

52 D. Makovec, B. Belec, T. Goršak, D. Lisjak, M. Komelj, G. Dražić, *et al.*, Discrete evolution of the crystal structure during the growth of Ba-hexaferrite nanoplatelets, *Nanoscale*, 2018, **10**(30), 14480–14491.

53 M. C. Zenobi, C. V. Luengo, M. J. Avena and E. H. Rueda, An ATR-FTIR study of different phosphonic acids adsorbed onto boehmite, *Spectrochim. Acta, Part A*, 2010, **75**(4), 1283–1288.

54 W. Gu, Q. Xie, C. Qi, L. Zhao and D. Wu, Phosphate removal using zinc ferrite synthesized through a facile solvothermal technique, *Powder Technol.*, 2016, **301**, 723–729.

55 N. Adden, L. J. Gamble, D. G. Castner, A. Hoffmann, G. Gross and H. Menzel, Phosphonic acid monolayers for binding of bioactive molecules to titanium surfaces, *Langmuir*, 2006, **22**(19), 8197–8204.

56 I. Řehoř, V. Kubíček, J. Kotek, P. Hermann, J. Száková and I. Lukeš, *Modification of Nanocrystalline TiO₂ with Phosphonate–and Bis (phosphonate)–Bearing Macrocyclic Complexes: Sorption and Stability Studies*, Wiley Online Library, 2011.

57 T. Daou, J. Grenèche, G. Pourroy, S. Buathong, A. Derory, C. Ulhaq-Bouillet, *et al.*, Coupling agent effect on magnetic properties of functionalized magnetite-based nanoparticles, *Chem. Mater.*, 2008, **20**(18), 5869–5875.

58 A. K. Yuen, G. A. Hutton, A. F. Masters and T. Maschmeyer, The interplay of catechol ligands with nanoparticulate iron oxides, *Dalton Trans.*, 2012, **41**(9), 2545–2559.

59 S. Čampelj, M. Pobrežnik, T. Landovsky, J. Kovač, L. Martin-Samos, V. Hamplova, *et al.*, The Influence of Catechols on the Magnetization of Iron Oxide Nanoparticles, *Nanomaterials*, 2023, **13**(12), 1822.

60 C. R. Vestal and Z. J. Zhang, Effects of surface coordination chemistry on the magnetic properties of MnFe₂O₄ spinel ferrite nanoparticles, *J. Am. Chem. Soc.*, 2003, **125**(32), 9828–9833.

61 Y. Sahoo, H. Pizem, T. Fried, D. Golodnitsky, L. Burstein, C. N. Sukenik, *et al.*, Alkyl phosphonate/phosphate coating on magnetite nanoparticles: a comparison with fatty acids, *Langmuir*, 2001, **17**(25), 7907–7911.

62 E. Keutner, Über Absorption in Dipolflüssigkeiten im Gebiet von 3–7 m Wellenlänge, *Ann. Phys.*, 1936, **419**(1), 29–48.

63 G. A. Seisenbaeva, I. V. Melnyk, N. Hedin, Y. Chen, P. Eriksson, E. Trzop, *et al.*, Molecular insight into the mode-of-action of phosphonate monolayers as active functions of hybrid metal oxide adsorbents. Case study in

sequestration of rare earth elements, *RSC Adv.*, 2015, **5**(31), 24575–24585.

64 F. G. Svensson, G. Daniel, C.-W. Tai, G. A. Seisenbaeva and V. G. Kessler, Titanium phosphonate oxo-alkoxide "clusters": solution stability and facile hydrolytic transformation into nano titania, *RSC Adv.*, 2020, **10**(12), 6873–6883.

65 X. Chen, E. Luais, N. Darwish, S. Ciampi, P. Thordarson and J. J. Gooding, Studies on the effect of solvents on self-assembled monolayers formed from organophosphonic acids on indium tin oxide, *Langmuir*, 2012, **28**(25), 9487–9495.

66 R. Kodama, Magnetic nanoparticles, *J. Magn. Magn. Mater.*, 1999, **200**(1–3), 359–372.

67 D. Makovec, M. Komelj, G. Dražić, B. Belec, T. Goršak, S. Gyergyek, *et al.*, Incorporation of Sc into the structure of barium-hexaferrite nanoplatelets and its extraordinary finite-size effect on the magnetic properties, *Acta Mater.*, 2019, **172**, 84–91.

68 G. A. Neff, C. J. Page, E. Meintjes, T. Tsuda, W.-C. Pilgrim, N. Roberts, *et al.*, Hydrolysis of surface-bound phosphonate esters for the self-assembly of multilayer films: Use of solid state magic angle spinning ^{31}p nmr as a probe of reactions on surfaces, *Langmuir*, 1996, **12**(2), 238–242.

69 F. Fairbrother, Nature, 160, 87 (1947), *J. Chem. Soc.*, 1948, 1051.

70 R. Guillien, La constante diélectrique au voisinage du point de fusion, *J. Phys. Radium*, 1940, **1**(1), 29–33.

71 R. Davies and T. T. Jones, XXVI. On the determination of the dielectric constants of liquids at radio frequencies.—Part III. Methyl alcohol, water, and alcohol water mixtures: Theoretical, *London, Edinburgh Dublin Philos. Mag. J. Sci.*, 1939, **28**(188), 289–306.